Thickness and fluctuations of free and adsorbed liquid films

Eva M. Fernández[*]
Instituto de Ciencia de Materiales de Madrid, CSIC, ES-28049, Madrid, Spain

Enrique Chacón[†]
Instituto de Ciencia de Materiales de Madrid, CSIC, ES-28049, Madrid, Spain and Instituto de Ciencia de Materiales Nicolás Cabrera, Universidad Autoñoma de Madrid, Madrid, ES-28049, Spain

Pedro Tarazona[‡]
Departamento de Física Teórica de la Materia Condensada, Universidad Autónoma de Madrid, Madrid, ES-28049, Spain and Instituto de Ciencia de Materiales Nicolás Cabrera, Universidad Autónoma de Madrid, Madrid, ES-28049, Spain

(Received 3 August 2011; revised manuscript received 20 October 2011; published 17 November 2011)

Effective mesoscopic Hamiltonians with the thickness of the adsorbed liquid films as a collective variable have been widely used in the study of adsorbed systems. In the present work, we show that the intrinsic surface of a liquid-vapor interface provides a very accurate way to evaluate the instantaneous film thickness in computer simulations. This film thickness follows with quantitative accuracy the predictions of simple model Hamiltonians, even for films as thin as one monolayer, and the effective interfacial potential has the simplest exponential form with a surprising accuracy, from a single monolayer to very thick films. For both the free liquid slabs and the adsorbed films and despite of the low vapor density, we have found that the fluctuations associated with the evaporation of particles to the vapor and their condensation in the liquid layer give an important contribution to the probability distributions of the liquid film thickness in our canonical (NVT) simulations.

DOI: 10.1103/PhysRevB.84.205435 PACS number(s): 68.08.Bc, 68.03.Hj, 68.03.Kn

I. INTRODUCTION

Effective Hamiltonian approaches have been used over the last decades to understand the basic phenomenology of adsorption systems, in particular, for fluids adsorbed on inert solid surfaces.[1] These models use the thickness of the adsorbed liquid film as a collective variable, and the free energy of the interfacial system is assumed to have a simple functional form in terms of the local film thickness $\xi(\mathbf{R})$ at each point on the $\mathbf{R} = (x, y)$ surface plane. Mean-field theories for wetting transitions[1,2] and dewetting dynamics[3] provide a qualitative understanding for the most salient features of these problems in terms of the mean film thickness $\langle\xi\rangle$. An effective surface Hamiltonian $\mathcal{H}[\xi(\mathbf{R})]$, for the analysis of the thickness fluctuations, is usually assumed to have two separated contributions: a local free energy $f[\xi(\mathbf{R})]$ per unit area plus the free-energy cost of the fluctuations at the films edge, described (as in the capillary wave theory for free liquid surfaces) through the surface tension, γ, multiplied by the area of the corrugated surface. However, in order to understand discrepancies between theory and computer simulations,[4,5] two nonlocal effective Hamiltonians have been proposed: the first one introduced the nonlocal effects in the interaction between the substrate and the liquid-vapor interface,[6,7] i.e., in the interface potential, while in the second one, the nonlocal effects are included replacing the interfacial tension by a position-dependent stiffness.[5] This second model may be recovered as a small gradient expansion of the first one, and it may create a stiffness instability at a wetting transition. The experimental validation of these hypothesis for the functional dependence of the effective surface Hamiltonian is very difficult, despite careful measurements of the disjoining pressure for large films,[8] because the experiments do not provide the resolution necessary to measure interfacial potentials for the required range of nanometer-thick films.

A promising alternative is to use computer simulations that may provide full information on the structures at molecular level. The calculation of coarse-grained free energies from simulation is a long standing problem that requires a computable link between the discrete molecular positions and the continuous mesoscopic variables like $\xi(\mathbf{R})$.[9,10] Effective Hamiltonians that use the macroscopic thermodynamic parameters, like the surface tension, may achieve a very accurate description of other related problems, like capillary condensation[11] and capillary wave fluctuations,[12–14] down to scales of about 10 molecular diameters. In that range, the results are fairly robust with respect to the specific choice to define the collective continuous parameters from the molecular positions.

In the range between 3 and 10 molecular diameters, the surface Hamiltonians may still be qualitatively correct, but quantitative accuracy requires the use of mesoscopic corrections, like a wave-vector dependence of the surface tension in the classical form of the capillary wave theory. In that case, the results may become strongly dependent on the specific choice of the projection of the molecular configurations into the collective mesoscopic variables like $\xi(\mathbf{R})$.[15,16] In the next section, we discuss two different ways to define the intrinsic surface for a free liquid-vapor interface that may be used to define the local thickness of an adsorbed liquid film. The usual recipe is based on the concept of the Gibbs dividing surface (GDS), and it defines the film directly from the total number of particles. The alternative procedure is the intrinsic sampling method (ISM) that localizes the edge of the liquid film and associates the film thickness to the volume between the surface and the substrate. The two proposals may

lead to different (nominal) fluctuations of the film thickness, and we explore here the relevance of those differences and their description in terms of effective Hamiltonians. The analysis is split in two steps: in Sec. III, we study free-standing liquid slabs coexisting with saturated vapor for which the only relevant variables are the volume and number of particles in each of the coexisting phases. In Sec. IV, we extend the analysis to films adsorbed on a planar substrate, to explore the form of the effective surface potential and its relevance for the fluctuations of the film thickness. This paper is restricted to the analysis of the mean film thickness, i.e., averaged over the whole surface with a simulation box of transverse size of about 10 molecular diameters. The implications for local fluctuations of the film are discussed in the final section together with the general conclusions for the limits of the computer simulation analysis in the validation of mesoscopic surface Hamiltonian models.

II. THE THICKNESS OF A LIQUID FILM

The usual description of adsorbed films from computer simulations is made through the density profile, $\rho(z) = \langle\hat{\rho}(z)\rangle$, given by the thermal equilibrium average ($\langle\ldots\rangle$) of the instantaneous density operator $\hat{\rho}(z) \equiv \sum_i \delta(z - z_i)\rangle/A_o$, where A_o is the area of the planar substrate, the coordinate z is perpendicular to it, and the index i runs over all the (fluid) particles. Liquid films adsorbed on solid surfaces usually show oscillatory (layering) structure in $\rho(z)$. For thin films, the layering structure goes directly down to the low-density vapor ρ_v, while for thick liquid layers, the density profile has a plateau with the liquid density, $\rho(z) \approx \rho_l$, between the structured solid-liquid region and the smooth decay of the density at the liquid-vapor edge of the film. Theoretical approaches have often used a specific value of the density profile [e.g., the middle value $\rho_e \equiv (\rho_l + \rho_v)/2$ or the 90–10 recipe $\rho_e \equiv 0.9\rho_l$] to define the position of the film edge at the value $z = z_e$ such that $\rho(z_e) = \rho_e$. The averaged film thickness is then defined as $\langle\xi\rangle = z_e - z_0$, i.e., the distance between the nominal edge and some (arbitrary) origin at the substrate.

Alternatively, the edge of the film may be defined as the GDS that sets the balance in the number of particles in $\rho(z)$ to be equivalent to a step function between the densities ρ_l and ρ_v. Assuming that all the N particles are contained in the interval $z_0 \leqslant z_0 + z \leqslant L_z$, this definition of the film thickness, ξ_N, reflects the total number of particles N enclosed in the simulation box:

$$\xi_N = \int_{z_0}^{z_0+L_z} dz \frac{[\rho(z) - \rho_v]}{(\rho_l - \rho_v)} = \frac{(N/A_o) - \rho_v L_z}{\rho_l - \rho_v}. \qquad (1)$$

The extensions of the above definitions to a local thickness $\xi(\mathbf{R})$ that represents the instantaneous shape of the adsorbed layer is often given for granted in theoretical analysis, assuming generic forms for the effective surface Hamiltonians $\mathcal{H}[\xi]$, independently of the specific definition of its functional variable. However, any attempt to extract the effective Hamiltonian from the computer simulations finds that the operational link between the molecular coordinates and the mesoscopic collective variable ξ is far from trivial. The self-averaging of the instantaneous density profile, $\hat{\rho}(z) \approx \langle\hat{\rho}(z)\rangle \equiv \rho(z)$ over a large transverse area A_0, makes the definition $\hat{\rho}(z_0 + \xi) = \rho_e$ for the thickness ξ, instantaneously averaged over the whole surface, very similar to its thermal average $\langle\xi\rangle$ defined from $\rho(z_0 + \xi) = \rho_e$; but the extension to a local thickness cannot be based on the full density distribution operator $\hat{\rho}(x,y,z)$ made by the sum of delta peaks at the instantaneous particle positions. Any definition of a smoothly corrugated local density distribution has to include some kind of coarse-graining, either in time or position, or both, and the local film thickness defined from $\rho[x,y,z_0 + \xi(x,y)] = \rho_e$ would incorporate the effects of such coarse graining into the effective surface Hamiltonian.

At first sight, the GDS definition for ξ_N may be more robust. In Eq. (1), we may replace N by the number of particles ΔN inside a small prism with basis of area ΔA parallel to the substrate around the point (x,y), and use ΔA instead of the total area A_o. This is to define the edge of the wetting layer as a local GDS, $\xi_N(x,y)$, and it has the appeal of being a conceptually simple recipe to compute the film thickness from the molecular positions. However, the application of this concept to the analysis of the capillary wave fluctuations on a free liquid surface leads to a complete failure when the size of the transverse sampling area ΔA becomes comparable to the molecular size. The bulklike fluctuations of the liquid density appear reflected as surface fluctuations, so that the nominal intrinsic surface $z = \xi_N(x,y)$, defined with this method, does not represent the instantaneous edge of the adsorbed film at molecular level.

To solve this problem, it was necessary to develop definitions of the intrinsic surface pinned to the surface, so that the effects of the bulk fluctuations could be eliminated. In these methods, the intrinsic surface $z = \xi(\mathbf{R})$ is linked to a set of molecules chosen to represent the instantaneous liquid surface, instead of relying on a density balance across the interface. The first proposal in this sense was made in 1985 by Stillinger,[17,18] but only over the last few years there has been a broad search for efficient and computationally feasible methods for the intrinsic sampling of fluid interfaces.[19–22] Here, we use the intrinsic sampling method (ISM)[15,16,23,24] based on the identification of N_s surface pivots among the instantaneous molecular positions. The number of such pivots per unit area, $n_s = N_s/A_0$, is used as a control parameter to get the sharpest resolution for the layering structure in the intrinsic density profile. The optimal value of n_s is interpreted as the two-dimensional density of the "outmost molecular layer" in a liquid surface; it depends on the molecular interactions and on the temperature, and it may be consistently determined from a wide range of structural and dynamical properties of the interface. We refer the reader to previous works[25] for a detailed discussion of this point. The only relevant point here is that the ISM provides an instantaneous shape for the intrinsic surface $z = \xi(x,y)$ that, applied to the edge of a wetting layer, defines the local thickness of a liquid film.

In the Fourier-space representation, $\xi(x,y) = \sum_q \hat{\xi}_q \exp[i(q_x x + q_y y)]$, the relevant variable for this work is the $q = 0$ component, $\hat{\xi}_0$, that may be used, instead of Eq. (1), as a collective variable to represent the thickness of the wetting layer $\xi_{\rm IS} = \hat{\xi}_0 - z_0$. The qualitative difference between ξ_N and $\xi_{\rm IS}$ is that the Gibbs dividing

surface method (1) relates the film thickness to the total number of particles, while the ISM gives a measure of the volume $\xi_{\rm IS}A_o$ occupied by the liquid film in each molecular configuration. Therefore along a canonical ensemble (NVT), the computer simulated ξ_N would be trivially constant while $\xi_{\rm IS}$ fluctuates. The aim of this paper is to explore the relation between these two variables, and the accuracy of mesoscopic effective Hamiltonians to describe the statistical properties of $\xi_{\rm IS}$.

III. FREE LIQUID SLABS

We consider a canonical ensemble simulation of a uniform liquid slab bounded by two (upper and lower) parallel liquid-vapor interfaces normal to the z direction. The system has a fixed number of particles N in a box of total volume $V = A_0 L_z$, and the usual GDS describes it as a slab of fixed width ξ_N given by Eq. (1) in terms of the bulk coexisting densities of the liquid and vapor phases. The number of molecules in the liquid and in the vapor are consistently fixed by $N_l = \rho_l A_0 \xi_N$ and $N_v = \rho_v A_0 (L_z - \xi_N) = N - N_l$. In contrast, the ISM identification of the liquid slab edges leads to a nominal thickness $\xi_{\rm IS} \equiv \hat{\xi}_0^{\rm sup} - \hat{\xi}_0^{\rm inf}$ that depends on the instantaneous molecular configuration. The number of particles within that volume may also change, so that we may consider a mesoscopic description of the system in which ξ and N_l are the variables of a free slab Hamiltonian $\mathcal{H}_{\rm slab}(\xi, N_l)$ that we model as

$$\mathcal{H}_{\rm slab}(\xi, N_l) = \xi A_0 f_l\left(\frac{N_l}{\xi A_0}\right) + (L_z - \xi) A_0 f_v\left[\frac{N - N_l}{(L_z - \xi)A_0}\right] + 2\gamma A_0, \quad (2)$$

where $f_l(\rho)$ and $f_v(\rho)$ are the free energies per unit volume in a bulk system when the density ρ is, respectively, near the fixed bulk coexisting values ρ_l and ρ_v. Assuming small density fluctuations around the thermodynamic equilibrium values, we use a second-order Taylor expansion to get

$$f_l(\rho) = -p_{lv} + \mu_{lv}\rho + \tfrac{1}{2}\mu_l'(\rho - \rho_l)^2, \quad (3)$$

and

$$f_v(\rho) = -p_{lv} + \mu_{lv}\rho + \tfrac{1}{2}\mu_v'(\rho - \rho_v)^2, \quad (4)$$

so that liquid and vapor bulk phases, with densities ρ_l and ρ_v, coexist with common pressure p_{lv} and chemical potential μ_{lv}, but different compressibilities, $\chi_l = 1/(\mu_l'\rho_l^2)$ and $\chi_v = 1/(\mu_l'\rho_v^2)$.

By construction, the minimum of $\mathcal{H}(\xi, N_l)$ with respect to the volume $A_0\xi$ and the number of particles N_l agrees with the GDS prescription, but Eq. (2) predicts finite fluctuations for these two variables. Within the usual Gaussian approximation for the probability distribution $\mathcal{P}(\xi, N_l) \propto \exp[-\beta\mathcal{H}(\xi, N_l)]$, the mean values of the slab thickness would be precisely at the minimum of $\mathcal{H}[\xi, N_l]$, i.e., at the GDS results $\langle\xi\rangle = \xi_N$ and $\langle N_l\rangle = \rho_l A_o \xi_N$. From the second-order derivatives of Eq. (2),

$$T_{xx} = \frac{\partial^2}{\partial\xi^2}\left(\frac{\mathcal{H}_{\rm slab}}{A_0}\right) = \frac{\mu_l'\rho_l^2}{\xi} + \frac{\mu_v'\rho_v^2}{L_z - \xi},$$
$$T_{xy} = A_0\frac{\partial^2}{\partial\xi\,\partial N_l}\left(\frac{\mathcal{H}_{\rm slab}}{A_0}\right) = -\frac{\mu_l'\rho_l}{\xi} - \frac{\mu_v'\rho_v}{L_z - \xi}, \quad (5)$$
$$T_{yy} = A_0^2\frac{\partial^2}{\partial N_l^2}\left(\frac{\mathcal{H}_{\rm slab}}{A_0}\right) = \frac{\mu_l'}{\xi} + \frac{\mu_v'}{L_z - \xi},$$

we get the mean square fluctuations of the thickness,

$$\langle\Delta\xi^2\rangle = \langle(\xi - \langle\xi\rangle)^2\rangle = \left[T_{xx} - \frac{T_{xy}^2}{T_{yy}}\right]^{-1} = \frac{\chi_l\rho_l^2\xi_N}{\beta A_o(\rho_l - \rho_v)^2} + \frac{\chi_v\rho_v^2(L_z - \xi_N)}{\beta A_o(\rho_l - \rho_v)^2}, \quad (6)$$

with two additive contributions proportional to the mean width of the liquid and vapor regions, ξ_N and $L_z - \xi_N$. We may use the ideal gas approximation for the vapor compressibility to estimate that $\chi_v\rho_v^2 \approx \beta\rho_v$ is much smaller than the prefactor $\chi_l\rho_l^2$ in the liquid contribution. However, for thin liquid films in large simulation boxes, $L_z \gg \xi$, the values of $\langle\Delta\xi^2\rangle$ with different amounts of vapor cannot be directly compared. This is due to the coupling between the fluctuations of ξ_N and N_l, given by the term T_{xy}^2/T_{yy} that represents the evaporation and condensation of molecules between the liquid and the vapor. In contrast, if we consider that the number of particles in the liquid is constant, the fluctuations of the slab thickness would be given by

$$\langle\Delta\xi^2\rangle = [T_{xx}]^{-1} = \left[\frac{\beta A_o}{\chi_l\xi_N} + \frac{\beta A_o}{\chi_v(L_z - \xi_N)}\right]^{-1}, \quad (7)$$

where the dependence on the box length L_z is qualitatively different than in Eq. (6), and it gives a well defined limit $\langle\Delta\xi^2\rangle = \chi_l\xi_N/(\beta A_o)$ for a very large thickness of the vapor region.

The point is that the canonical ensemble for the whole system, with N particles in a fixed volume V, is not a canonical ensemble for the liquid slab. The vapor phase provides a finite reservoir of particles that may condensate in (or evaporate from) the liquid. In the limit when the volume occupied by the vapor, $A_0(L_z - \xi_N)$, is very large, the liquid slab would be effectively in a grand canonical (μVT) ensemble at the chemical potential of liquid-vapor coexistence with very large fluctuations in its thickness. Only if the vapor is very rarefied or its volume is not too large, we may expect that $\chi_v\rho_v^2(L_z - \xi_N) \approx \beta\rho_v(L_z - \xi_N) \ll \chi_l\rho_l^2\xi_N$ so that the second term in Eq. (6) may be neglected, and the difference with Eq. (7) is reduced to the factor $\rho_l^2/(\rho_l - \rho_v)^2 \approx 1$, since we approach the critical point $\rho_v \ll \rho_l - \rho_v \approx \rho_l$.

The application of the ISM to the free surfaces of the liquid slab allows us to check the method, comparing the simulation results with the above predictions of the effective Hamiltonian (2). The first question is the accuracy of the prediction $\langle\xi_{\rm IS}\rangle = \xi_N$, so that the mean volume occupied by the liquid, $\xi_{\rm IS}A_0$, equals the thermodynamic value given by the GDS. To check this point, we have run molecular dynamics (MD) simulations with an Lennard-Jones (LJ) potential fluid, truncated at $r_c = 2.5\sigma$, at temperature $k_bT = 0.75\epsilon$, in terms

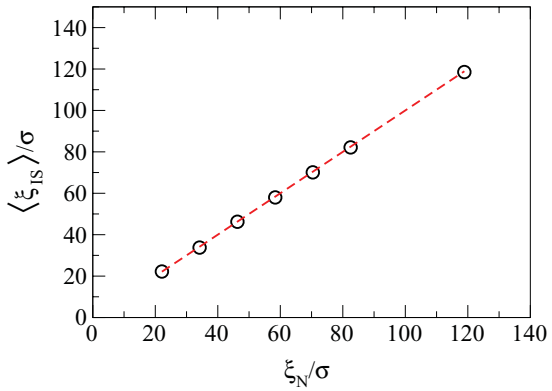

FIG. 1. (Color online) Circles: liquid-film thickness of the free liquid slab (NVT simulation) evaluated with the ISM recipe $\langle \xi_{IS} \rangle$ against its Gibbs dividing surface value ξ_N. Dashed line: theoretical behavior giving by $\langle \xi \rangle = \xi_N$.

of the usual LJ parameters σ and ϵ. The transverse dimensions of the box (with periodic boundary conditions) are always the same, $L_x = L_y = 10.457\sigma$, while the longitudinal size L_z is changed, between $L_z = 110\sigma$ and 260σ, to accommodate liquid slabs of different thickness, at equilibrium with its vapor. Canonical ensemble simulations were carried with $N = 2000$ to 10 000 particles, and the coexisting liquid-vapor densities $\rho_l = 0.7598\sigma^3$ and $\rho_v = 0.0126\sigma^3$ were obtained with samplings restricted to regions well inside the liquid and vapor phases. Using these values, the nominal slab thickness ξ_N given by the GDS in Eq. (1) is constant for all the configurations along any simulation with fixed N.

The ISM procedure was used to obtain the instantaneous intrinsic surface associated to the upper and lower edges of the slab, with samplings over 10 000 configurations, separated by 500 time steps and after 4000 time steps for equilibration. The instantaneous values of the $q = 0$ Fourier component were used to get the slab thickness $\xi_{IS} = \hat{\xi}_0^{sup} - \hat{\xi}_0^{inf}$, and they give the mean values $\langle \xi_{IS} \rangle$ represented in Fig. 1 for different values of ξ_N (i.e., different total number of particles). The surface density of pivot molecules used in the ISM algorithm was kept equal to the optimal value $n_s = 0.7/\sigma^2$ for the free LJ liquid surface at this temperature.[25] The results show that the ISM identification of the liquid volume is very precise, the linear fit to the points in Fig. 1 gives $\langle \xi_{IS} \rangle = 0.9966\xi_N - 0.05\sigma$, so that the slope is within 0.4% of its nominal value, well within the accuracy for the independent determination of the coexisting densities ρ_l and ρ_v that determine ξ_N in Eq. (1). What is still more relevant is the small mismatch at the origin: the volume within the two ISM surfaces is accurate at the level of 0.05 molecular diameters per unit transverse area. Therefore the estimation of the slab thickness given by the ISM offers an extremely precise link between the molecular structure of the system and its thermodynamic description.

The fluctuations of ξ_{IS} obtained along the NVT-MD simulation may be directly compared with the prediction of the effective mesoscopic Hamiltonian (2) to check the relevance of the two contributions in Eq. (6). In the top panel of Fig. 2, we present the mean squared fluctuations of ξ_{IS} for a slab with $\xi_N = 50\sigma$ and with several cell sizes L_z. The number of particles was changed, between 4237 and 4443 to keep

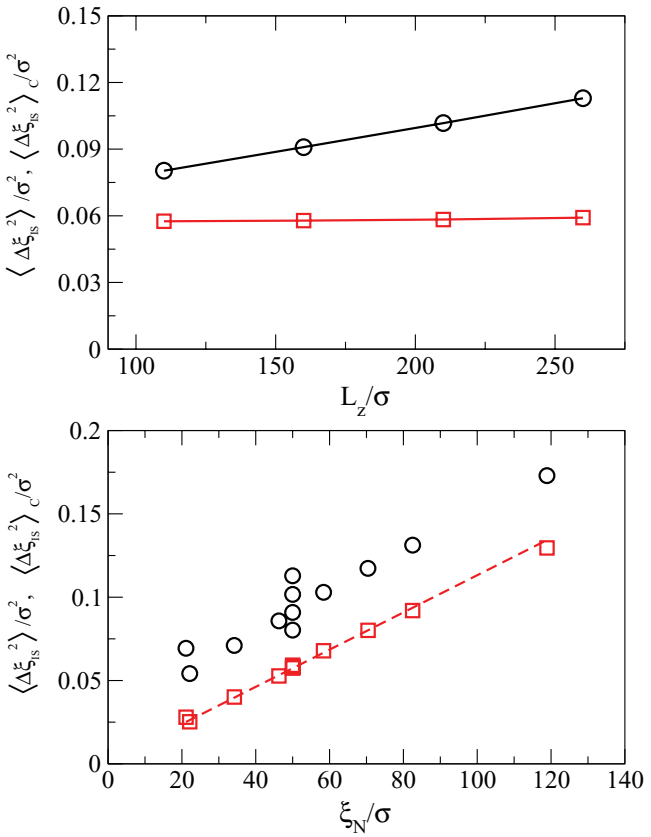

FIG. 2. (Color online) Fluctuations of the free liquid slab thickness: (black) circles are the simulation values $\langle \Delta\xi_{IS}^2 \rangle$ and the (red) squares the canonical values $\langle \Delta\xi_{IS}^2 \rangle_C$ obtained after removing the effect of the vapor slab. Top panel: fluctuations of a liquid slab with fixed GDS width $\xi_N = 50\sigma$ at coexistence with vapor slabs of different sizes $L_z - \xi_N$. Lower panel: fluctuations for different liquid ξ_N and vapor slab thickness. In the lower panel, the (red) dashed line shows the fit to Eq. (6).

constant ξ_N. We see that our simulations verify the theoretical prediction (6) that predicts an affine increase of $\langle \Delta\xi_{IS}^2 \rangle$ with the cell size L_z. This result confirms the importance of the evaporation and condensation of particles between the liquid and the vapor phases in the evaluation of $\langle \Delta\xi_{IS}^2 \rangle$. From the slope of the line, we can get the compressibility of the vapor, $\chi_v = 83.48\beta\sigma^3/\epsilon$, slightly above its ideal gas value $\chi_v = \beta/\rho_v = 79.36\beta\sigma^3/\epsilon$.

We may define an effective canonical amplitude for the fluctuations of the liquid slab through the extrapolation of $\langle \Delta\xi \rangle^2$ to null amount of vapor (i.e., to $L_z = \langle \xi \rangle$),

$$\langle \Delta\xi^2 \rangle_C = \langle \Delta\xi^2 \rangle - \frac{\partial \langle \Delta\xi^2 \rangle}{\partial L_z} (L_z - \langle \xi \rangle), \tag{8}$$

that corresponds to the first term in Eq. (6). The results for $\langle \Delta\xi_{IS}^2 \rangle_C$ presented by the squares in Fig. 2 are indeed independent of the amount of vapor. The lower panel of the same figure presents the results as a function of ξ_N, to show that the values of $\langle \Delta\xi_{IS}^2 \rangle$ for different L_z (circles) collapse in a single straight line for $\langle \Delta\xi_{IS}^2 \rangle_C$, consistently with the first term in Eq. (6). From the slope of this line and using the previously given values for the coexisting densities, we may extract the value $\chi_l = (0.14 \pm 0.01)\beta\sigma^3/\epsilon$ for the compressibility of the

coexisting liquid phase. This value is compatible with the value obtained by calculating the density fluctuations in the center of the slab, $\chi_l = (0.13 \pm 0.01)\beta\sigma^3/\epsilon$.

The good linear fits in both panels of Fig. 2 support the validity of the ISM estimation for the slab thickness as the relevant mesoscopic variable for the effective Hamiltonian (2). It is important to remark that the LJ model, at $k_bT = 0.75\epsilon$, and the range of cell sizes used in our simulations are representative of typical computer simulation studies for adsorbed liquid films. Under these conditions, the evaporation and condensation of particles from one phase to the other play a relevant role, since we observe a clear increase in the fluctuations with the box length L_z, that should be taken into account to compare simulations made in different boxes. Taking the effective canonical ensemble for the liquid slab, the fluctuations are reduced but still we get $\sqrt{\langle \Delta\xi_{\rm IS}^2 \rangle_{\rm C}} \sim 0.2\sigma$ to 0.4σ, clearly above the accuracy for the ISM determination of that thickness. Therefore the compression expansion of the coexisting phases is observed in NVT simulations run with typical models and sizes, and they should be taken into account if we aim to link effective Hamiltonians, like Eq. (2), with the probability distribution for the film thickness extracted from computer simulations. Finally, note that for our computer simulations, the width of the liquid-vapor interface is mainly determined by the capillary fluctuations (ξ_q with $q > 0$), and the fluctuations of the $q = 0$ term analyzed here would only become relevant for slabs thicker than 200σ.

IV. ADSORBED FILMS

In this section, we apply the ISM to determine the thickness of adsorbed liquid layers on a solid substrate. In order to simplify the problem, we consider only a situation of complete wetting over a structureless substrate. The substrate is modeled as a planar wall at $z = 0$, which acts on the fluid as an external potential $V_{\rm sf}(z)$ that depends only on the distance to the wall plane. In particular, we use a sum over three layers with truncated 4–10 potentials cut at $r_c = 2.5\sigma_{\rm sf}$,

$$\frac{V_{\rm sf}(z)}{8\pi\epsilon_{\rm sf}\sigma_{\rm sf}\rho_{\rm lay}} = \sum_{i=1}^{3}\left\{\left[\frac{1}{10}\left(\frac{\sigma_{\rm sf}}{(z-z_i)}\right)^{10} + \frac{1}{4}\left(\frac{\sigma_{\rm sf}}{(z-z_i)}\right)^{4}\right] - \left[\frac{1}{10}\left(\frac{\sigma_{\rm sf}}{r_c}\right)^{10} - \frac{1}{4}\left(\frac{\sigma_{\rm sf}}{r_c}\right)^{4}\right]\right\}, \quad (9)$$

with LJ parameters $\epsilon_{\rm sf} = 1.3$, $\sigma_{\rm sf} = 0.912\sigma$ for the solid-fluid interactions, and with $\rho_{\rm lay} = 1.143\,\sigma^2$ as the density in each layer. This model potential has been previously used by Velasco *et al.*,[26,27] and it gives complete wetting by the LJ liquid at the temperature $k_bT/\epsilon = 0.75$ used here. A purely repulsive potential is considered at $z = L_z$, to close the simulation cell along the Z axis, with the usual periodic boundary conditions on the X and Y directions.

A. NVT simulations

We have run series of canonical ensemble Monte Carlo simulations with $N = 150$ to 2000 LJ particles, to analyze adsorbed films up to a thickness of 23.5σ in a simulation box with $L_x = L_y = 10.457\sigma$ and $L_z = 65.36\sigma$. The systems were equilibrated for about 2.5 ns (5×10^5 time steps) and the production time was 20 ns (4×10^6 time steps) with a time step of 5 fs. The ISM was applied, as in the previous section, to get now the intrinsic surface associated to the external edge of the adsorbed film, and we take as the measure of the film thickness the difference, $\xi_{\rm IS} = \hat{\xi}_0 - z_0$, between the $q = 0$ Fourier component of the intrinsic surface and a fixed position z_0 to represent the inner edge of the film, close to the solid-substrate edge. The surface density of pivot molecules used in the ISM algorithm was kept equal to the optimal value for the free liquid films considered in the previous section.

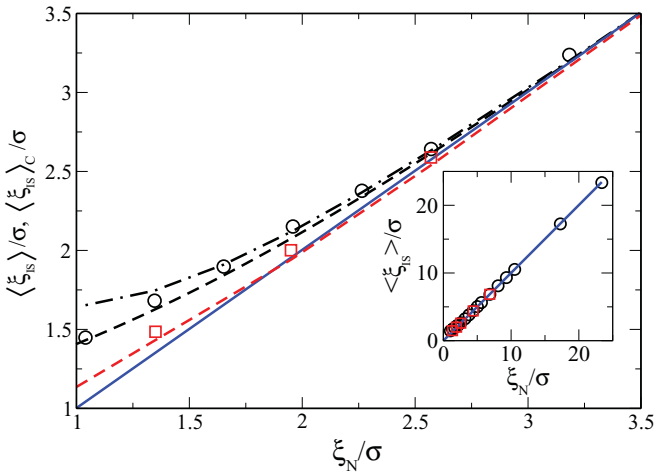

FIG. 3. (Color online) Liquid-film thickness of adsorbed films calculated by the ISM $\langle\xi_{\rm IS}\rangle$ vs the GDS thickness. (Black) Circles are the simulation values $\langle\xi_{\rm IS}\rangle$ and the (red) squares the canonical values $\langle\xi_{\rm IS}\rangle_{\rm C}$ obtained after removing the effect of the vapor slab and given by Eq. (10). The dashed lines are the exact theoretical values obtained by numerical minimization of the mesoscopic Hamiltonian (19), and the dashed-dotted line is the analytical approximation to linear order in the effective potential for $\langle\xi_{\rm IS}\rangle$ given by Eq. (20). The (blue) full line is the free slab behavior giving by $\langle\xi\rangle = \xi_N$.

Figure 3 presents the mean ISM thickness $\langle\xi_{\rm IS}\rangle$, from canonical MD simulations with different number of particles, given in terms of the GDS thickness ξ_N. For thick films, our results show that $\langle\xi_{\rm IS}\rangle$ recovers the unit slope with respect to ξ_N as we have checked for free liquid slabs. The nominal position for the inner edge of the film has been fixed to be $z_0 = 0.67\sigma$, with respect to the position of the outer solid layer in Eq. (9). This choice makes $\langle\xi_{\rm IS}\rangle = \xi_N$ for thick films (see full line and the figure inset), and it corresponds to the zero-adsorption GDS for the solid-liquid interface. The difference between $\langle\xi_{\rm IS}\rangle$ and ξ_N appears only for thin adsorbed films, with less than three molecular layers, for which the mean ISM values deviates upward with respect to the asymptotic straight line. This effect depends on the box size L_z and it reflects the difference between the density of the saturated vapor ρ_v used in Eq. (1) and the actual density of the undersaturated vapor at equilibrium with a thin film. Therefore there are less molecules in the vapor and the film is thicker than its nominal GDS value, $\langle\xi_{\rm IS}\rangle \geqslant \xi_N$. This effect could be eliminated if the definition for ξ_N includes the actual value of $\rho_v(N/A_0, L_z)$, measured from the bulk vapor density in the simulations, but the value would depend on the solid-fluid interaction potential $V_{\rm sf}(z)$, and this

prediction requires a theoretical approach at molecular level. An alternative for the direct analysis of the MD simulations is to compare the results for $\langle \xi_{IS} \rangle$ with several box sizes L_z and to extrapolate them to the value $L_z = \langle \xi \rangle$, which corresponds to the effective canonical limit for the liquid film, as analyzed for the fluctuations of the free slabs in the previous section:

$$\langle \xi \rangle_C = \langle \xi \rangle - \frac{\partial \langle \xi \rangle}{\partial L_z}(L_z - \langle \xi \rangle). \tag{10}$$

The results of this extrapolation are given by the squares in Fig. 3, and they are much closer to the asymptotic line than the circles, which represent the raw results for a typical box size $L_z = 65.36\sigma$. The small residual deviation from $\langle \xi_{IS} \rangle_C = \xi_N$ describes that thin films (with $\xi_N \lesssim 1.5\sigma$) are slightly less dense than thick liquid films, so that their volume $A_0 \xi_{IS}$ is slightly larger than that of the same number of particles in the liquid bulk. Again, this is a microscopic effect that produces small variations in the value of the "mesoscopic" film thickness, depending on its molecular definition. Even if we avoid the effects of the vapor volume, taking the $L_z = \langle \xi_{IS} \rangle$ limit, we may observe some differences between the GDS definition, based on the number of particles, and the ISM definition based on the film volume.

The fluctuations of the film thickness are shown in Fig. 4. As for the free liquid slab studied in the previous section, the size L_z of the simulation box is a most relevant variable for $\langle \Delta \xi_{IS}^2 \rangle$, since with the typical values of the vapor density and the simulation box size, the fluctuations associated with the evaporation and condensation of particles are as large as those given by the compression and expansion of the adsorbed film. We may get the same effective canonical ensemble limit, $\langle \Delta \xi_{IS}^2 \rangle_C$, taking the extrapolation of the results to $L_z = \langle \xi_{IS} \rangle$. As in the results for $\langle \xi_{IS} \rangle$, the fluctuations of the film thickness reflect also a clear change at $\xi_N \approx 3\sigma$. Above this value, the fluctuations grow with the film thickness exactly as the free liquid slabs studied in the previous section, with the slope given by Eq. (6) in terms of the density and compressibility of the two bulk coexisting phases. For thin films with $\xi_N \lesssim 3\sigma$, the mean-square fluctuations of the thickness decay below the asymptotic straight line, again, an effect that can only be predicted with a description at molecular level.

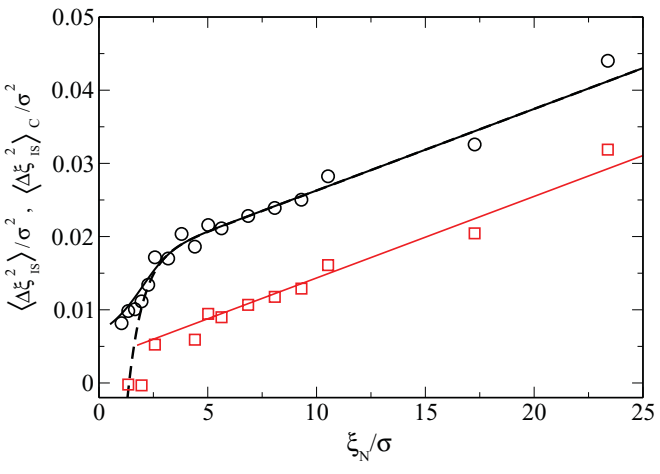

FIG. 4. (Color online) Fluctuations in the intrinsic surface of adsorbed films vs the GDS thickness ξ_N. Circles are the simulation values $\langle \Delta \xi_{IS}^2 \rangle$ and the squares its canonical values $\langle \Delta \xi_{IS}^2 \rangle_C$ obtained after removing the effect of the vapor slab. The solid lines are the values obtained from the exact numerical second-order derivatives of the mesoscopic Hamiltonian (19), and the dashed line is the analytical approximation to linear order in the effective potential of $\langle \Delta \xi_{IS}^2 \rangle$ given by Eq. (21).

B. Mesoscopic Hamiltonians

Mesoscopic Hamiltonians for the local thickness $\xi(x,y)$ of adsorbed layers are usually written with the functional form:

$$\begin{aligned} &\frac{1}{A_0}\mathcal{H}[\xi(x,y)] \\ &\quad = \frac{1}{A_0}\int dxdy[f(\xi(x,y)) + \gamma\sqrt{1+|\nabla\xi(x,y)|^2} - \gamma] \\ &\quad \approx f(\hat{\xi}_0 - z_0) + \frac{1}{2}\sum_q [f''(\hat{\xi}_0) + \gamma q^2]|\hat{\xi}_q|^2 + \cdots, \end{aligned} \tag{11}$$

were $f(\xi)$ is the free energy per unit area of a film with uniform thickness ξ. This function is evaluated at the local value of the film thickness, $\xi(x,y)$, over the whole substrate area. The other contribution is proportional to the surface tension γ of the liquid-vapor interface, to account for the corrugations at the outer edge of the liquid film. The third line in Eq. (11) expands $\mathcal{H}[\xi]$ up to quadratic order in the Fourier components of the local thickness.

In the present work, we are restricted to the study of the effective Hamiltonian for the instantaneous film thickness averaged over the whole area A_0, $\xi \equiv \hat{\xi}_0 - z_0$, which is given by the local free energy $f(\xi)$,

$$\frac{1}{A_0}\mathcal{H}[\xi] = f(\xi), \tag{12}$$

that may be obtained from the probability distribution for the mean film thickness $\mathcal{P}(\xi) \sim \exp[-\beta\mathcal{H}[\xi]]$, sampled along computer simulations. Therefore the function $f(\xi) = -\ln[\mathcal{P}(\xi)/(\beta A_0)] + C$ may be obtained, except for an additive constant. This $f(\xi)$ depends on the statistical ensemble of $\mathcal{P}(\xi)$ and also on the definition of the mesoscopic variable ξ. We use $\mathcal{P}(\xi|N)$ for the canonical ensemble probability with N particles and $\mathcal{P}(\xi|\mu)$ for the grand canonical ensemble with chemical potential μ. Although we do not make it explicit, the probabilities would also depend on the temperature T as well as on the box dimensions, $A_0(= L_x L_y)$ and L_z.

The GDS definition $\xi = \xi_N$ in Eq. (1) gives a constant film thickness along any canonical ensemble simulation ξ, so that $\mathcal{P}(\xi|N) = \delta(\xi - \xi_N)$. In contrast, the ISM definition allows the fluctuations of ξ, so that the probability distribution $\mathcal{P}(\xi|N) \propto \exp[-\beta A_0 f(\xi|N)]$ is a Gaussian defined by the mean value $\langle \xi \rangle$ and the mean-square deviation $\langle \Delta \xi^2 \rangle$ described above. The dependence of these Gaussian parameters on the size of the simulation box reflects the role of the vapor as a finite particle reservoir. A very large vapor volume would act as a grand-canonical reservoir of particles for the liquid film, and the function $f(\xi|N)$ becomes the grand-potential energy of the adsorbed film, $f(\xi|\mu)$, with the chemical potential μ as the only relevant parameter.

As the chemical potential approaches the liquid-vapor coexistence value, the wetting layer grows, and the grand canonical probability $\mathcal{P}(\xi|\mu)$ is spread over the whole box length, $0 \lesssim \xi \lesssim L_z$. For undersaturated systems, $\Delta\mu \equiv \mu_{lv} - \mu > 0$, the probability for thick films decays exponentially like $\exp(-\beta\Delta\mu N)$ and the excess of particles in the film goes like $(\rho_l - \rho_v)A_0\xi$, so that the free energy for large thickness grows like $f(\xi) \approx \Delta\mu(\rho_l - \rho_v)\xi$. At the opposite limit, for thin films, the attraction of the fluid toward the substrate creates an effective repulsion of the liquid-vapor edge of the film that is represented by an effective potential $\Phi(\xi)$ decaying to zero for thick films, and assumed to be independent of $\Delta\mu$,

$$f(\xi|\mu) = \Phi(\xi) + \Delta\mu\left[\frac{N(\xi)}{A_0} - L_z\rho_v\right] = \Phi(\xi) + \Delta\mu\,(\rho_l - \rho_v)\,\xi. \quad (13)$$

Therefore we can define the effective potential $\Phi(\xi)$ as the free energy per unit area of a liquid film with uniform thickness ξ at coexistence with its vapor:

$$\Phi(\xi) = f(\xi|\mu_{lv}) = -\ln[\mathcal{P}(\xi|\mu_{lv})/(\beta A_0)] + C, \quad (14)$$

where the constant C, tied to the normalization of $\mathcal{P}(\xi|\mu)$, is fixed to get $\Phi(\xi) = 0$ for large ξ. Notice that $\Phi(\xi)$ may depend on the specific definition of film thickness, so that the GDS and the ISM estimates for ξ, could lead to different effective potentials.

C. The effective potential $\Phi(\xi)$ from restricted μVT simulation

For short-ranged interactions, as the truncated LJ potential used here, a generic density functional analysis[28] predicts the asymptotic exponential decay $\Phi(\xi) \sim \exp(-\lambda\xi)$, where λ may be obtained from the decay of the density profile toward the liquid bulk, $\rho_l - \rho(z) \sim \exp(-\lambda z)$. The Landau-Ginzburg density approximation gives (shorter range) corrections to the pure exponential decay of the potential with terms like

$$\Phi(\xi) = \Phi_o e^{-\lambda\xi} + \Phi_1 e^{-2\lambda\xi} + \cdots \quad (15)$$

that become relevant for the analysis of the possible nonlocal effects.[6,7]

We do not know the general range of validity for the asymptotic form (15), but it is often assumed that the film has to be thicker than 3–4 molecular layers, to avoid the interference between the layering structure of $\rho(z)$ near the substrate and the external edge of the liquid layer. On the other hand, the analysis of computer simulations results could only settle the discussion on the alternative and subtle corrections over the simple Hamiltonian form (11) if the effects are observable close to the wall where the effective potential $\Phi(\xi)$ is observable above the noise level of the simulation.

The sampling of $\mathcal{P}(\xi|\mu)$ near saturation requires extremely large simulation times to get good statistics over a wide range of film thickness. Moreover, small differences in the chemical potential, like $\beta\Delta\mu \sim \pm 0.01$, produce enormous changes in the probability for observing a film with $\xi \sim 10\sigma$, with factors $10^{\pm 10}$ in a simulation box with $A_0 = 100\sigma^2$. In order to overcome these difficulties, we have used a variant of the known umbrella sampling technique, the successive sampling, developed recently by L.G. McDowell and M. Muller.[10,29] The successive sampling procedure performs a grand canonical Monte Carlo simulation restricted to consecutive intervals $[N_{i-1}, N_i]$ in the allowed number of particles. Monte Carlo simulations are performed in each interval and moves that try to leave the interval are rejected. The restricted probability distributions $P_i(N|\mu)$ for the number of particles and $P_i(\xi|\mu)$ for the film thickness are calculated in each interval, and the results at neighbor intervals are matched at their boundary, with free fitting parameters $F_i(\mu)$, to get a continuous form:

$$P(N|\mu) = F_i(\mu)P_i(N), \quad N \in [N_{i-1}, N_i]. \quad (16)$$

We may (arbitrarily) take $F_1 = 1$, and then

$$F_i(\mu) = \frac{\prod_{j=0}^{j=i} P_{j-1}(N_{j-1}|\mu)}{\prod_{j=0}^{j=i} P_j(N_{j-1}|\mu)}\; i \neq 1, \quad (17)$$

gives the (unnormalized) probability distribution, like those presented in Fig. 5 for two values of the chemical potential close to the saturation value $\beta\mu = -8.3774$ and -8.2940. We have used intervals with $N_i - N_{i-1} = 30$ in a simulation box with $L_x = L_y = 10.457\sigma$ and $L_z = 65.36\sigma$. The systems were equilibrated for about 2.5 ns (5×10^5 time steps) and the production time was 20 ns (4×10^6 time steps) with a time step of 5 fs.

Notice that the functions in Fig. 5 span over a huge range $\sim 10^{10}$ of relative values. The precise determination of $P(N|\mu)$ over such range would be impossible with an unrestricted grand-canonical sampling, since a good sampling of the less probable regions would require an unfeasible long simulation time mostly spent in the most probable regions. Moreover, the method may be used both above and below the saturation value $\mu = \mu_{lv}$, as shown by the slopes of the two curves in Fig. 5 at large N. The precise value $\beta\mu_{lv} = -8.3065$ may be obtained by interpolation between the slopes of the two dashed lines.

The values of $F_i(\mu)$ obtained from Eq. (17) may be also used to get the (unnormalized) probabilities for the film thickness, $P(\xi|\mu) = F_i(\mu)P_i(\xi|\mu)$, either with the GDS definition ξ_N

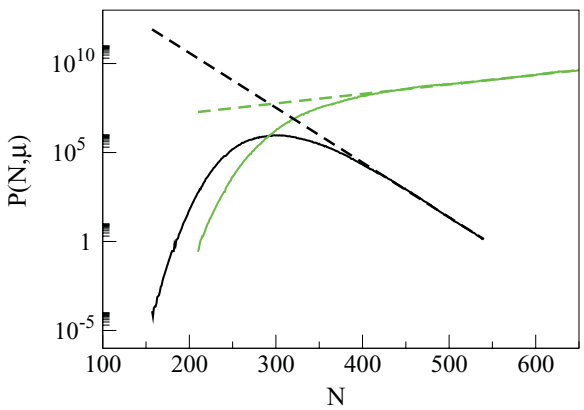

FIG. 5. (Color online) Probability distributions for the number of particles $P(N,\mu)$ obtained from restricted μVT simulations at two different chemical potentials. The dashed lines show the exponential fit to large values of N. Dark (black) lines: results for $\beta\mu = -8.3774$. Light (green) lines: results for $\beta\mu = -8.2940$.

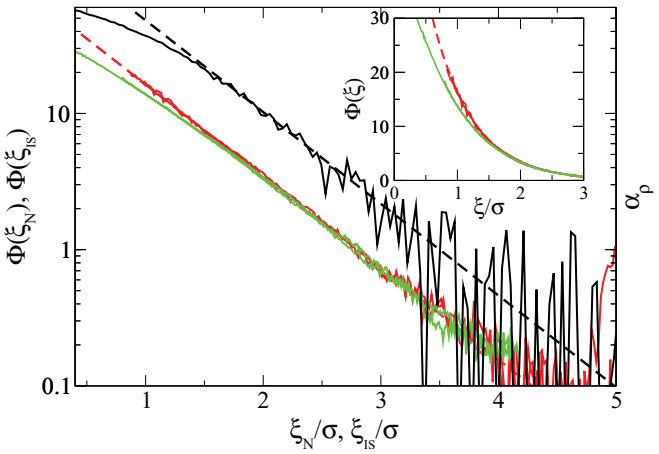

FIG. 6. (Color online) The lower curves are the interfacial potentials $\Phi(\xi)$ obtained from the probability distributions. The dark (red) full curves are $\Phi(\xi_{\rm IS})$ as a function of ISM thickness of the slab $\xi_{\rm IS}$, and the light (green) curves are $\Phi(\xi_N)$ as a function of ξ_N, i.e., of the total number of particles N. In both cases, we show the results for the two chemical potentials simulated, $\beta\mu = -8.3774$ and -8.2940, although the curves are indistinguishable. The dashed line shows the exponential fit to the curve $\Phi(\xi_{\rm IS})$. The upper (black) curves show the asymptotic decay of the density profile (α_ρ) in the liquid-vapor interface and its exponential fit (dashed line). The inset shows $\Phi(\xi_{\rm IS})$ and ξ_N with linear axis scale.

(that is a linear transformation of N) or with the ISM results $\xi = \xi_{\rm IS}$. The effective wall potential is directly extracted as

$$\Phi(\xi) \equiv -\frac{1}{\beta A_0}\ln\left[\frac{P(\xi|\mu_{lv})}{P(\xi_{\max}|\mu_{lv})}\right] \approx -\frac{1}{\beta A_0}\ln\left[\frac{P(\xi|\mu)e^{\beta\Delta\mu N}}{P(\xi_{\max}|\mu)e^{\beta\Delta\mu N_{\max}}}\right]. \quad (18)$$

The results for both the GDS $\Phi(\xi_N)$ and the ISM $\Phi(\xi_{\rm IS})$ are presented in Fig. 6. In both cases, the difference between the estimations done from positive and negative $\Delta\mu$ are well below the noise level, supporting the splitting of $f(\xi)$ in Eq. (13) as a linear term proportional to $\Delta\mu$ plus a decaying wall potential $\Phi(\xi)$. The most remarkable aspect of the effective potential obtained with the ISM definition of $\xi_{\rm IS}$ is observed in the main panel of Fig. 6. Within the accuracy of our simulations, we get a perfect exponential form, with $\beta\Phi_o = 215.4/\sigma^2$. The exponential decay $\lambda = 1.55/\sigma$ is the same as observed in the asymptotic decay of the density profile in the free liquid-vapor interface, as predicted by the asymptotic density functional analysis for the true correlation length,[28,30] so that all the relevant aspects of the solid-fluid interaction are represented by the value of the prefactor Φ_o.

The simple matching procedure (17) is not accurate enough to get $\Phi(\xi_{\rm IS})$ over the simulation noise for $\xi \gtrsim 4\sigma$. However, we may reasonably assume that the pure exponential continues for larger $\xi_{\rm IS}$ and use it to determine the parameters $F_i(\mu)$, with the excellent piecewise matching of the continuous function $\Phi(\xi_{\rm IS})$, for the full range explored in Fig. 6. The surprising simplicity of $\Phi(\xi_{\rm IS})$, from a single monolayer to very thick films, contrasts with the strong layering structure of the density profiles shown in Fig. 7 that would suggest a more complex relation between the film thickness and its

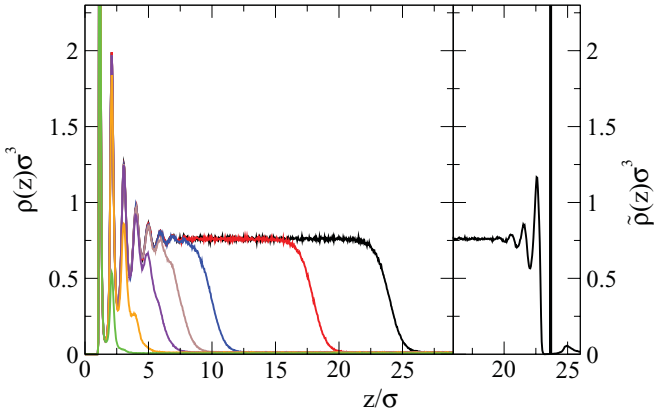

FIG. 7. (Color online) The left panel shows the density profiles of the adsorbed fluid for several total numbers of particles $N =$ 2000, 1500, 850, 650, 500, 325, and 150. The right panel shows the intrinsic density profile for the thicker film $N = 2000$.

free energy. Also, it is surprising to not find any $\sim\exp(-2\lambda\xi)$ terms that are predicted by density functional approximations for $\mathcal{H}[\xi]$,[6] with the definition of the film thickness associated to a given value of the (assumed smooth) local density profile, $\rho[x,y,z_0+\xi(x,y)] = \rho_e$. Such terms are, indeed, observed in the density profile and also in effective potential $\Phi(\xi_N)$ associated to the GDS definition of the film thickness, as shown in Fig. 6.

We may assume that the deviation of $\Phi(\xi_N)$ from the pure exponential form is produced by the same causes that produce the flattening of the function $\langle\xi_{\rm IS}\rangle(\xi_N)$ for thin films. The GDS definition for ξ_N describes the film thickness in terms of the total number of particles, letting aside the fact that a thin film would be at equilibrium with an undersaturated vapor, and that only for thick wetting layers the vapor phase would approach saturation.

D. Theoretical results

As discussed above, if we want to develop a theoretical model to describe our simulation NVT of the adsorbed liquid films, we must take into account the role of the vapor as a finite particle reservoir. So we must keep the double dependence on the volume, $A_0\xi$, and the number of particles in the liquid film N_l used at the study of the free slab (2), instead of a single variable, either ξ or ξ_N, used at mesoscopic Hamiltonians (11) developed in order to study adsorbed films in the grand-canonical ensemble. We may generalize the effective Hamiltonian (2) to include the effect of the solid substrate with the form

$$\mathcal{H}(\xi,N_l) = \mathcal{H}_{\rm slab}(\xi,N_l) + \frac{N_l}{\xi(\rho_l-\rho_v)}\Phi(\xi) = \mathcal{H}_{\rm slab}(\xi,N_l) + \frac{N_l\Phi_o}{\xi(\rho_l-\rho_v)}e^{-\lambda\xi}, \quad (19)$$

Notice that Φ_o is the only information on the substrate-fluid interactions included in Eq. (19). The parameters ρ_l, ρ_v, μ_l', μ_v', and λ contain all the relevant information on the coexisting fluid phases, and they are independent of the solid substrate. The remaining parameters in Eqs. (2) and (19) are the geometry of the system given by the transverse area A_0 and the length

L_z. As we have observed in the description of the simulation results, despite its low density, the role of the vapor phase as a finite reservoir for the adsorbed film is important, and it produces a dependence of $\langle\xi\rangle$ and $\langle\Delta\xi^2\rangle$ with L_z that has to be taken into account for the analysis of simulation results. The exploration of the mesoscopic Hamiltonian (19), and the comparison of its results with the simulation data in Figs. 3 and 4, allow to check the interpretation given above for the role of the evaporation and condensation processes in adsorbed liquid layers.

To that effect, the minimization of Eq. (19) under the canonical ensemble constrain (i.e., for fixed ξ_N) may be done analytically up to linear order in Φ_o, to get

$$\langle\xi\rangle = \xi_N - \frac{\Phi_0\rho_l}{(\rho_l-\rho_v)^3}\big\{\chi_l\rho_l^2[1-(1+\lambda\xi_N)e^{-\lambda\xi_N}] - \rho_l\rho_v\chi_l(1-e^{-\lambda\xi_N}) - \chi_v\rho_v^2\lambda(L_z-\xi_N)e^{-\lambda\xi_N}\big\}, \quad (20)$$

where the first term, ξ_N is the mean width that would have the free slab of N_l particles without the presence of the wall. For an adsorbed film, the free slab thickness is changed by the second term, which includes both the increase due to the undersaturation of the vapor for small thickness and the (always small) difference between the mean density of the film $N_l/(\xi_N A_0)$ and the bulk liquid density ρ_l. As shown by the dashed-dotted lines in Fig. 3, the result of Eq. (20) is in agreement with the MD results for $\langle\xi_{\rm IS}\rangle$ at the range $\xi_N \gtrsim 1.7\sigma$, the deviation for thinner films is due to the linear expansion on Φ_o, since the full numerical minimization of $\mathcal{H}(\xi, N_l)$ produces very good agreement over the full range thickness explored here, i.e., from a monolayer film (see dashed line in Fig. 3). As in the analysis of the simulation results, we may cancel the evaporation effects through the extrapolation of the results to $L_z = \langle\xi\rangle$, i.e., with an effective canonical ensemble for the liquid film. Again, the prediction of the mesoscopic Hamiltonian (19) is in excellent agreement with the simulation results $\langle\xi_{\rm IS}\rangle_{\rm C}$, proving that the results of the ISM definition for the thickness of adsorbed liquid layers in computer simulations may be described by a simple mesoscopic Hamiltonian with a very high resolution (better than a tenth of the molecular diameter).

In the same way, we obtain the fluctuations of the thickness of the adsorbed through the second derivatives of the free energy. Again we have to solve theset equations numerically but the analytical first-order approximation is achievable:

$$\begin{aligned}\langle\Delta\xi^2\rangle = {} & \frac{\chi_l\rho_l^2\xi_N + \chi_v\rho_v^2(L_z-\xi_N)}{\beta A_0(\rho_l-\rho_v)^2} - \frac{\phi_0\rho_l}{\beta A_0(\rho_l-\rho_v)^5} \\ & \times\big(\chi_l^2\rho_l^4\big\{1-[1+\lambda\xi_N-(\lambda\xi_N)^2]e^{-\lambda\xi_N}\big\} \\ & -\rho_l^3\rho_v\chi_l^2[1-(1-2\lambda\xi_N)e^{-\lambda\xi_N}] \\ & +\rho_l^2\rho_v^2\chi_l\chi_v\{1+[-1+\lambda(L_z-4\xi_N) \\ & -2\lambda^2\xi_N(L_z-\xi_N)]e^{-\lambda\xi_N}\} \\ & +\rho_l\rho_v^3\chi_l\chi_v\{1-[1+2\lambda(L_z-\xi_N)]e^{-\lambda\xi_N}\} \\ & +\chi_v^2\rho_v^4\lambda(L_z-\xi_N)[3+\lambda(L_z-\xi_N)]e^{-\lambda\xi_N}\big). \quad (21)\end{aligned}$$

The results are shown in Fig. 4, again compared with the numerical full minimization of (19) that extends the good agreement with the simulation results over the entire range of film thickness.

V. SUMMARY AND CONCLUSIONS

The aim of this paper is to explore the application of the ISM, to define the thickness of adsorbed layers on solid substrates. The method, developed for the analysis of capillary wave fluctuations in free liquid surfaces, defines the instantaneous volume of the film per unit transverse area, $\xi = V_{\rm film}/A_0$, rather than the usual Gibbs dividing surface definition of the film thickness ξ_N, directly related to the total number of particles in the system. The analysis of free liquid slabs with two parallel liquid-vapor interfaces has been compared with the predictions of a mesoscopic Hamiltonian in which the coexisting phases are treated as fluctuating volumes with fluctuating densities under the canonical constrain of fixed total number of particles and total volume. The excellent agreement obtained in that comparison proves that the ISM results represent the volume of free liquid slabs with a precision better than a tenth of the molecular diameter σ. With that assurance, we have gone to the application of the ISM for adsorbed layers in which we could foresee major difficulties, due to the strong layering structure of the density profiles $\rho(z)$. It is usually assumed that such effective Hamiltonians $\mathcal{H}[\xi]$ could only describe thick adsorbed layers, when the profile presents a plateau $\rho(z) \approx \rho_l$ between the layered region near the substrate, and the liquid-vapor interface at the outer edge of the film. However, our main result here is that the ISM results for ξ follow very precisely the predictions of simple model Hamiltonians, even for films as thin as one monolayer.

The obvious advantage of this outcome is that the sampling of molecular configurations, along computer simulations of adsorbed layers, may be accurately used to get the effective interfacial potential $\Phi(\xi)$ for the film thickness. If the mesoscopic description were restricted to very thick films, for which this potential is already very small, it would be impossible to extract precise information from the intrinsic noise of the simulation results. However, since the method works well also for thin films for which $\Phi(\xi) \gtrsim 20kT/\sigma^2$, the functional form of this mesoscopic potential may be obtained very accurately. Thus we establish a quantitative link between realistic models for solid-fluid interfaces and the generic mesoscopic Hamiltonians used to describe the behavior of these systems at large scale.

Moreover, the form of the thickness potential is particularly simple: over the whole range $\sigma \lesssim \xi \lesssim 5\sigma$ for which we get accurate results this effective potential follows the predicted asymptotic form $\Phi(\xi) = \Phi_0\exp(-\lambda\xi)$, with the same decaying constant λ observed in the tail of the density profile toward the liquid bulk, and with the constant Φ_0 as the only parameter to reflect the effects of the solid-fluid interactions. Such simplicity for $\Phi(\xi)$ goes even beyond what is usually assumed in model mesoscopic Hamiltonians $\mathcal{H}[\xi]$, obtained from the theoretical analysis with mean-field density functional techniques, that predict $\exp(-2\lambda\xi)$ corrections for thin films. The analysis of computer simulations for other temperatures and molecular models would be needed to know if the result obtained here is general, or if there is some fortuitous simplification of $\Phi(\xi)$ for the particular system simulated here. In particular, a pure exponential decay could appear in tricritical wetting transitions.[31] We are currently investigating the wetting behavior of the model to check this possibility.

A simple model Hamiltonian, which makes use of the thermodynamic data for the coexisting fluid phases and takes Φ_o as the only simulation result from the solid substrate, gives an excellent representation of the probability distributions for the film thickness. It is important to notice that such good quantitative agreement is achieved only if we allow the fluctuations of both the film volume and its mean density (or the number of particles that it contains). As in the case of the free liquid slabs, the fluctuations associated with the evaporation of particles to the vapor and their condensation in the liquid layer, give an important effect to the volume of the simulation box occupied by the vapor phase. This effect has to be taken into account when comparing simulations with different sizes, and we have shown how it may be eliminated through an extrapolation to the "effective canonical" ensemble for the liquid film.

On the other hand, we may wonder how a simple model, based on the treatment of the adsorbed film as a uniform liquid slab, is so accurate in the description of strongly layered density profiles. A possible answer is that the layering of the fluid near the wall reflects its short-range correlation structure, but changing it very little, so that both the entropic and energetic effects of the fluid-fluid interactions are really similar to those in a bulk liquid. This interpretation is supported by the view of the fluid interface obtained through the intrinsic density profile in Fig. 7, which shows the strong layering at the free edge of the film, rather than at the substrate side. The difference between the mean $\rho(z)$ and the intrinsic $\tilde{\rho}(z)$ profiles is just a matter of "reference system" to fix the origin of z; in the first case, it is tied to the rigid substrate, while in the second it is tied to the instantaneous position of the fluctuating free edge of the liquid film, but both profiles describe the same reality, a distribution of highly correlated particles that may in fact be much more similar to a homogeneous liquid bulk than what could be guessed from its density profiles.

Finally, in this work, we have addressed only the effective Hamiltonian for the instantaneous film thickness averaged over the whole area A_0 of the substrate. The grand-canonical prediction for $\Phi(\xi)$ is one of the key ingredients to plug into the effective Hamiltonian $\mathcal{H}[\xi(x,y)]$ like Eq. (2) that describes the fluctuations of the local thickness on each point of the interface. The second contribution is given by the fluctuations of the free edge of the film, treated as a liquid surface, and the ISM was precisely designed to that effect, i.e., to open a quantitative connection between computer simulations of liquid surfaces and the capillary wave theory (CWT). In that respect, it has been clearly established that the simple CWT Hamiltonian based on the macroscopic surface tension fails for wave vectors $q \gtrsim 1/\sigma$. The distribution of amplitudes for the intrinsic surface Fourier components $\hat{\xi}_q$ is still Gaussian, but their mean-square values are given by $\langle|\hat{\xi}_q|^2\rangle = kT/[A_0 q^2 \gamma(q)]$, with a wave-vector-dependent surface tension that only goes to its macroscopic limit for low q. This fact is particularly important since the alternative proposals for the relevant form of $\mathcal{H}[\xi(x,y)]$ are centered in the effects of the solid substrate on the fluctuations of the film thickness, and they may be understood as alternative proposals for a q-dependent correction over the classical CWT Hamiltonian. The fact that even for the free liquid interface there are important deviations of $\gamma(q)$ from its macroscopic limit $\gamma(0)$ sets a new perspective to analyze the possible relevance of the alternative proposals for realistic systems. A very recent publication by Pang *et al.*[32] has presented evidence in favor of the nonlocal interface model for the Ising model. Work in progress addressing these questions would be reported in a future publication.

ACKNOWLEDGMENTS

We acknowledge the support of the Spanish Minister of Science and Innovation (Grant No. FIS2010-22047-C05) and the Comunidad Autónoma de Madrid under program MODELICO (Grant No. S2009/ESP-1691).

*efernand@icmm.csic.es
†echacon@icmm.csic.es
‡pedro.tarazona@uam.es

[1] D. Bonn, J. Eggers, J. Indekeu, J. Meunier, and E. Rolley, Rev. Mod. Phys. **81**, 739 (2009).
[2] M. Schick, *Introduction to wetting phenomena* (Elsevier Science Publishers, 1990).
[3] U. Thiele, M. G. Velarde, and K. Neuffer, Phys. Rev. Lett. **87**, 016104 (2001).
[4] S. Dietrich, in *Phase Transition and Critical Phenomena*, edited by C. Domb and J. Lebowitz (Academic, New York, 1988), Vol. 12, pp. 1–218.
[5] M. E. Fisher and A. J. Jin, Phys. Rev. Lett. **69**, 792 (1992).
[6] A. O. Parry, J. Phys. Condens. Matter **8**, 10761 (1996).
[7] A. O. Parry, C. Rascón, N. R. Bernardino, and J. M. Romero-Enrique, Phys. Rev. Lett. **100**, 136105 (2008).
[8] R. Seemann, S. Herminghaus, and K. Jacobs, J. Phys. Condens. Matter **13**, 4925 (2001).
[9] K. Binder, Z. Phys. B **43**, 119 (1981).
[10] L. G. MacDowell and M. Müller, J. Chem. Phys. **124**, 084907 (2006).
[11] R. Evans and P. Tarazona, Phys. Rev. Lett. **52**, 557 (1984).
[12] F. P. Buff, R. A. Lovett, and F. H. Stillinger, Phys. Rev. Lett. **15**, 621 (1965).
[13] R. Evans, Adv. Phys. **28**, 143 (1979).
[14] J. Percus, in *Fluid Interfacial Phenomena*, edited by C. Croxton (Wiley, New York, 1986), pp. 1–44.
[15] E. Chacón and P. Tarazona, Phys. Rev. Lett. **91**, 166103 (2003).
[16] P. Tarazona and E. Chacón, Phys. Rev. B **70**, 235407 (2004).
[17] F. H. Stillinger, J. Chem. Phys. **76**, 1087 (1982).
[18] F. Stillinger and J. Weeks, J. Chem. Phys. **99**, 2807 (1995).
[19] J. Chowdhary and B. M. Ladanyi, J. Phys. Chem. B **110** (31), 15442 (2006).
[20] L. B. Pártay, G. Hantal, P. Jedlovszky, A. Vincze, and G. Horvai, J. Comput. Chem. **29**, 945 (2008).

[21]D. Zhukhovitskii, J. Chem. Phys. **125**, 234701 (2007).
[22]M. Jorge and M. Cordeiro, J. Phys. Chem. C **111**, 17612 (2008).
[23]E. Chacón and P. Tarazona, J. Phys. Condens. Matter **117**, S3493 (2005).
[24]F. Bresme, E. Chacón, and P. Tarazona, Phys. Chem. Chem. Phys. **10**, 4704 (2008).
[25]E. Chacón, E. M. Fernández, D. Duque, R. Delgado-Buscalioni, and P. Tarazona, Phys. Rev. B **80**, 195403 (2009).
[26]E. Velasco and P. Tarazona, J. Chem. Phys. **91**, 7916 (1989).
[27]E. Velasco and P. Tarazona, Surf. Sci. **251**, 628 (1991).
[28]R. Evans, J. R. Henderson, D. C. Hoyle, D. A. Parry, and Z. A. Sabeur, Mol. Phys. **80**, 755 (1993).
[29]L. M. MacDowell and M. Müller, J. Phys. Condens. Matter **17**, S3523 (2005).
[30]R. Evans, D. C. Hoyle, and A. O. Parry, Phys. Rev. A **45**, 3823 (1992).
[31]A. O. Parry, C. Rascón, and J. M. Romero-Enrique, J. Phys. Condens. Matter **19**, 416105 (2007).
[32]L. Pang, D. P. Landau, and K. Binder, Phys. Rev. Lett. **106**, 236102 (2011).